A SPAD-based linear sensor with in-pixel temporal pattern detection for interference and background rejection with smart readout scheme

Alessandro Tontini*†, Leonardo Gasparini†, Roberto Passerone*
*University of Trento, via Sommarive 9, 38123 Trento, Italy
†Fondazione Bruno Kessler, via Sommarive 18, 38123 Trento, Italy
Email: tontini@fbk.eu; gasparini@fbk.eu; roberto.passerone@unitn.it

***Abstract*—In this work, a 1x64 pixel SPAD-based linear sensor for direct time-of-flight (d-ToF) applications with real-time in-pixel interference and background rejection is presented. Each pixel is composed by 4 SPADs with passive quenching, a digital logic circuit to exploit photon temporal coincidence with a threshold of up to 3 photons for background rejection, a finite state machine for the detection of temporal laser patterns for the rejection of interfering signals generated by other similar devices and a 16-b time-to-digital converter with 150 ps timing resolution that can be repurposed for intensity measurements. The sensor implements a smart readout scheme capable to output only pixels with meaningful data, i.e., detection events that have been validated by the photon temporal coincidence circuit and/or the laser pattern detection circuit.**

***Index Terms*—Single Photon Avalanche Diode (SPAD), Light Detection And Ranging (LiDAR), direct time-of-flight (d-ToF).**

I. Introduction and related work

3D sensing-capable devices are widespread in several fields, from the industry to the consumer market. Among the many techniques that provide depth information, direct time-of-flight (d-ToF) with SPADs implemented in CMOS technology proved to be one of the most promising, thanks to the integration capability of the most advanced process nodes. Among the many challenges that SPAD-based CMOS d-ToF sensors have to face, dealing with background light and interference from similar devices are currently the limiting factors.

Background light rejection has been extensively studied and several techniques proved to be effective, such as photon temporal coincidence [1], time-gated acquisitions [2] or, for long-distance targets, the detection of the last incoming photons [3]. On the other hand, with the rapid diffusion of such devices, the need to deploy solutions for mutual interference suppression is capturing the attention of researchers even more than background light, especially in autonomous-driving scenarios.

Notable works provided effective solutions to reduce the disturbance effect from unwanted laser sources. Ximenes et al. [4] implemented a phase-shift keying (PSK) modulation on the emitted laser pulse, thus spreading interference sources below the level of the signal of interest. Seo et al. [5] exploit interference suppression by means of the emission of two laser pulses, whose timing signature is recognized and used to reject any other source with a different temporal pattern.

Both approaches demonstrated their effectiveness in reducing the effect of interference. With a PSK modulation of the emitted laser pulse [4], interference is not eliminated, but only attenuated, where the efficiency of attenuation depends on the number of phase shifts of the modulation. On the other hand, it has the advantage of requiring only one laser pulse, as opposed to the second approach, where two laser pulses with a known timing signature are emitted [5]. This approach, however, allows for a complete cancellation of interfering sources, as unknown detections are eliminated rather than attenuated. In the work from Seo et al. [5], this technique is exploited in post-processing over the collected histogram of timestamps with promising results.

In this work, we present a 1x64 pixel SPAD-based linear sensor embedding in-pixel background and interference rejection, with a smart readout scheme capable of selecting only pixels containing validated data to improve the sensor rate of operation. The interference rejection is based on the emission of two laser pulses with a known timing signature as in [5], but in this work it is implemented directly on a pixel basis in a compact form and operates in real time, thus no post-processing is required on the histogram of timestamps. The benefit of an active, in-pixel interference rejection is twofold. First, also background light can be rejected, resulting in an increased signal to background ratio in the final histogram. Second, power consumption is reduced as the TDC is activated only when two photon detections occur within the expected time frame, resulting also more robust against pile-up distortion, as the probability of saturating the TDC channel is reduced.

The paper is organized as follows. A detailed description of the array architecture is provided in Section II, focusing in particular on the pixel architecture (Section II-A) and on the readout scheme (Section II-B). Characterization results are reported in Section III, while conclusions and perspectives for future improvements are discussed in Section IV.

II. Architecture

In this section, we describe the sensor in detail, focusing on the pixel architecture and on the readout scheme.

A. Pixel architecture

The pixel, designed in a 110 nm 4M CIS technology, is composed by 4 SPADs arranged as a mini digital silicon photomultiplier. Each SPAD is passively quenched by 2 thick-oxide transistors to recharge the SPAD and properly clamp the voltage to 1.2 V to be compliant with the following circuitry. Each SPAD is paired with a monostable circuit to create a temporal window for the coincidence detection circuit, which is realized in pure digital logic. A threshold of N=1/4, N=2/4 and N=3/4 events can be selected via SPI programming. The output from the coincidence detection is fed into the measurement control circuit, which implements a finite state machine for the detection of the laser signature. The laser temporal signature can be set with 4-bit granularity, i.e., up to 16 combinations are possible. The TDC is based on a fine-coarse architecture, where the coarse timing measurement is given by an 8-bit counter with 100 MHz clock and the fine timing by a ring oscillator with 150 ps timing resolution. The TDC 8-bit counter can be repurposed to count the number of detected photons for intensity measurements. When the sensor is operated to recognize the laser pattern to reject interference, the TDC is triggered only when the second laser pulse is correctly detected, reducing unnecessary power consumption.

The measurement control circuit generates a *VALID* flag whenever a photon-detection event occurs. If the laser pattern detection feature is disabled, a *VALID* flag is generated by the first incoming event, which can be either the first detected photon (if no coincidence threshold is applied) or the first 2 or 3 photons detected within the coincidence window generated by the monostable circuit. The *VALID* flag is needed by the smart readout scheme to optimize the bandwidth by reading only pixels with validated data.

The chip micrograph, array architecture and pixel block diagram are shown in Figure 1.

B. Readout architecture

With the capability to exploit both the photon coincidence and laser signature detection, a reduction in the amount of generated data is expected. For this reason, a classical scheme where the entire array is read out is not optimized, as pixels with either non-validated data or background data are anyway considered, resulting in an increased readout time, negatively affecting the sensor frame rate. For this reason, we implemented a dedicated readout circuit which is able to output only pixels with meaningful data, i.e., detection events that have been validated by the photon coincidence circuit and/or the finite state machine for the detection of the temporal laser pattern. The readout process comprises two phases: the first phase is meant to transfer 1 bit per pixel to inform the controller FPGA about which pixels contain valid data. In the second phase, only pixels with validated data are read out, thus suppressing zeros. The first readout phase is therefore only needed for the controller FPGA to associate each data values with the pixels that generated it, with a minimum overhead of only 1 bit per pixel.

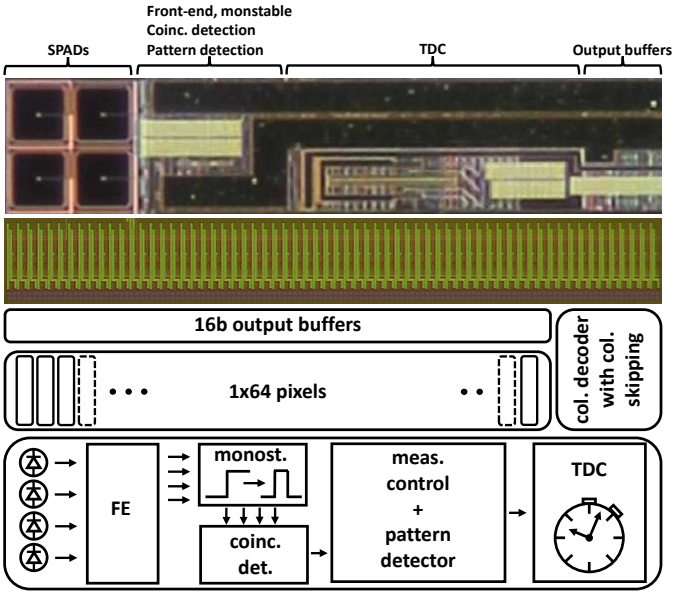

Fig. 1. Chip micrograph, array architecture and pixel block diagram. The array of pixels is implemented in a 110 nm 4M CIS technology within a multi-project chip. Due to the reuse of the TDC from a previous project, pixel size is not optimized, resulting in a final pitch of 40 x 180 μm^2. The in-pixel measurement control block, with laser signature detection capability, has an area occupation of 28 x 14 μm^2. By considering the device from Manuzzato et al., [3], which is realized in the same technology node with a pixel pitch of 48 x 48 μm^2, the occupation of this block takes 17% of the total pixel area, thus allowing its integration also in a 2D array.

The proposed readout scheme well matches with the in-pixel implementation of the laser signature detection, as the generation of data from the sensor can be highly reduced with such a strong filtering. Consequently, the benefit in terms of performance is twofold: on one side, the reliability of the timestamp detected with the in-pixel finite state machine for the laser pattern detection is increased, and on the other side the reduced amount of data (mainly due to the filtered events) results in a decrease of the required readout time, with benefits in terms of frame rate and power consumption.

III. Characterization

In this section, characterization results focusing on the in-pixel laser pattern detection and readout circuit performance are shown.

A. In-pixel laser pattern detection characterization

The in-pixel laser pattern detection feature has been first characterized on a single pixel basis using only the coarse TDC (100 MHz counter) information by means of two low-power picosecond pulsed lasers. The first laser was meant to be the signal source, while the second was used as an interferer. A picture describing the experimental setup is shown in Figure 2. The sensor is operated in the presence of background light, without any optical bandpass filter in front of the detector and with a coincidence threshold of N=2 photons. The results of the first characterization are shown in Figure 3, demonstrating that an interference with a histogram peak 18.5 dB higher than

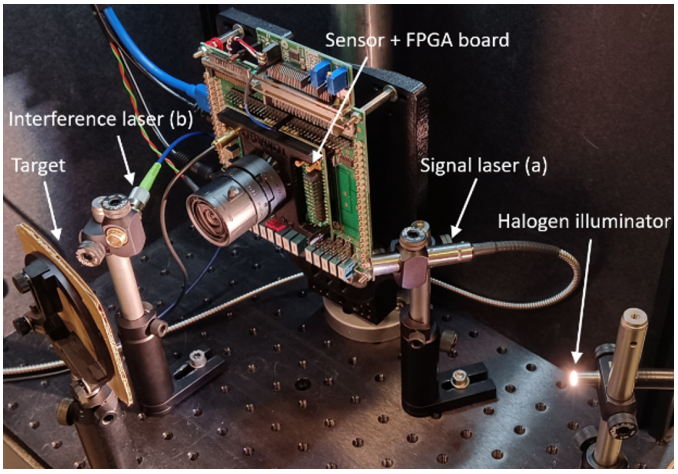

Fig. 2. Picture of the experimental setup to test the in-pixel interference-rejection capability with the signal laser (a) and the interfering laser (b). Each laser has been set with its own timing signature: for the signal of interest, the two laser pulses are separated 80 ns from each other, while for the interfering signal the pulses separation is 90 ns.

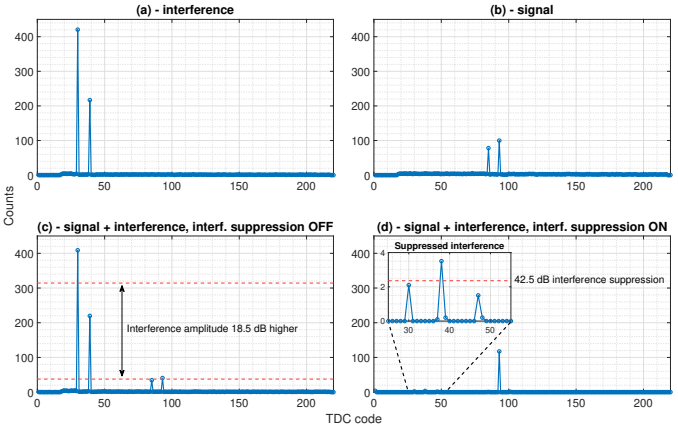

Fig. 3. First experimental validation of the interference-rejection capability of the device. Histograms (a) and (b) show the contribution of interference (a) and signal (b) alone, while in (c) the joint effect of the two sources is shown (with laser signature detection disabled). To stress the interference-rejection capability, the interference histogram peak is 18.5 dB higher in amplitude than the peak of the signal of interest. When the in-pixel interference-rejection is enabled (d), the interfering signal is almost completely suppressed by 42.5 dB, whereas the signal of interest gains 10 dB with respect to case (c), enabling the possibility to build an interference-free histogram directly from pixel data.

the signal of interest is almost completely eliminated, with a suppression of 42.5 dB. On the other hand, the signal of interest gained 10 dB with respect to the case where no laser pattern matching detection was applied, demonstrating that the in-pixel active detection of laser temporal patterns also helps in reducing uncorrelated background light.

Then, the entire array has been characterized with the 3D measurement of a scene profile, using the fine resolution given by the 150 ps in-pixel ring-oscillator and employing two 25 W 905 nm lasers for the emission of the temporal laser pattern. A third laser was pointed toward a portion of the scene, to emulate the interference from a second device. Results are shown in Figure 4.

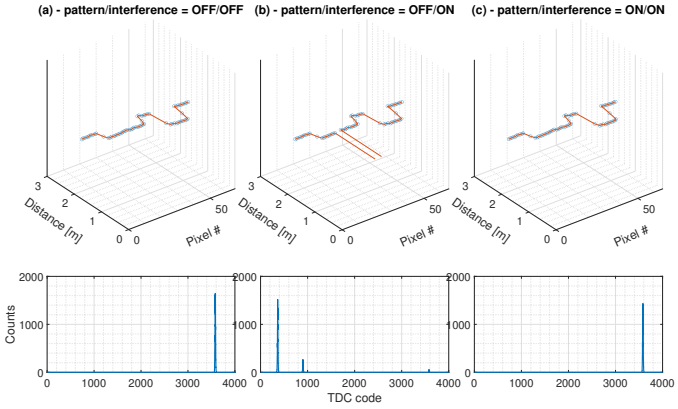

Fig. 4. Measurement of the profile of a scene composed by 2 boxes with different size and distance (range 0-2m). The first measurement (a) is a reference obtained without any interfering signal and with pattern detection disabled. In the second measurement (b), the interfering laser is pointed toward the first box with an earlier timing with respect to the signal laser, resulting in a complete loss of information from the illuminated portion of the target. In the third measurement (c), the in-pixel laser pattern detection was enabled allowing for a complete recovering of the lost information, as the interfering laser timestamps are actively discarded in favor of the signal laser timestamps, which have the correct timing. For each measurement, the histogram of one pixel under the interfering portion of the target is shown.

With a third measurement we targeted the background-rejection capability of the sensor by focusing on the combination between the photon coincidence technique and the in-pixel laser pattern detection. The sensor was operated without optical bandpass filter and a 180 W halogen illuminator was used to flood the scene with background photons. Without any background/interference rejection features, it was impossible to reconstruct the 3D profile of the scene. The 3D information was recovered completely with the photon coincidence technique (operated with a threshold of N=2/4 photons), but still several background events are allowed to trigger a coincidence, increasing the amount of data generated by the sensor and thus the required readout time. By enabling the laser pattern detection on top of the photon coincidence, it was anyway possible to reconstruct the 3D profile of the scene and at the same time dramatically reduce the amount of false triggers, with a reduction of data of $\simeq 98\%$ with respect to the previous case. By considering the laser peak to background ratio of the histogram, the combination of the laser pattern matching on top of the photon coincidence detection allowed to gain $\simeq 23$ dB, thus increasing the robustness of the measurement. Results are shown in Figure 5.

B. Readout performance assessment

The readout architecture has been characterized in two ways. The first characterization aimed at showing the capability of the sensor to output only pixels with meaningful data. For this measurement, a target (flat panel) was illuminated completely by background light and a collimated laser source was used to illuminate only a portion of it, resulting in only 2 pixels of the array to be shined with laser photons. First, no background-rejection technique was applied nor laser pattern

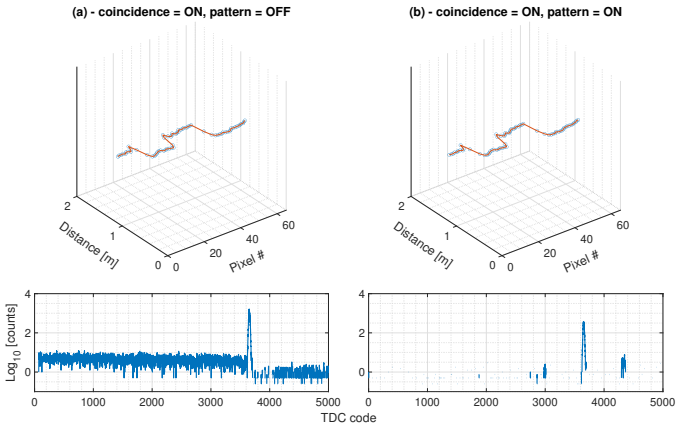

Fig. 5. Measurement of the 3D profile of a scene with high background light. In (a), only the photon coincidence technique was enabled, with a threshold of N=2/4 photons. In (b), the laser pattern detection was enabled on top of the photon coincidence, resulting in $\simeq$ 98% data reduction with respect to (a). The laser peak to background ratio is $\simeq$ 50 dB in (a) and increased up to $\simeq$ 73 dB in (b).

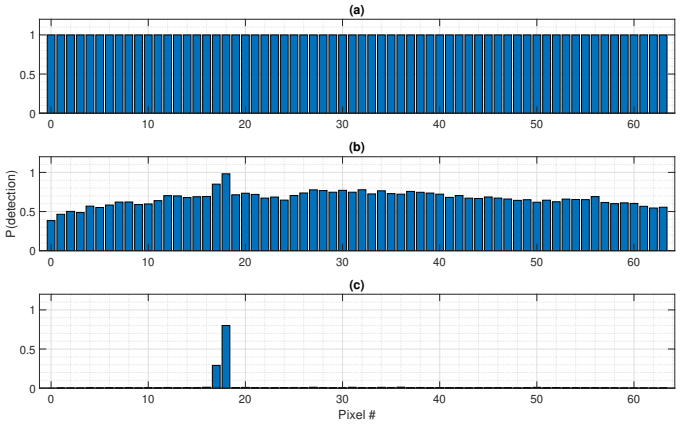

Fig. 6. Measured per-pixel activity (in terms of probability of detection) with the proposed readout scheme. With a minimum 1-bit overhead per pixel, it is possible to output only pixels with validated data. In (a), the readout ratio is almost 100% as no data filtering technique was applied. In (b), the enabling of the photon coincidence technique allows to reduce the readout ratio down to 66%, with a visible readout peak activity over pixels number 17 and 18, as they coincide with the reflected laser footprint. In (c), the additional enabling of the in-pixel laser pattern matching detection allows to recover the information from the only two illuminated pixels, further reducing the readout ratio down to a minimum of 2.25%.

matching detection, resulting in a probability of detection of almost 1 for all pixels. Then, photon coincidence detection was enabled with a threshold of N=2 photons, and a general reduction of the probability of detection is observed, but still allowing background-only pixels to be triggered. In the last measurement, the in-pixel laser pattern detection was enabled on top of the photon coincidence, reducing the probability of detection on pixels not illuminated by the laser source to a negligible level, allowing to only output data from the subset of pixels illuminated by the laser. Results are shown in Figure 6.

In the second characterization, only background light was considered and the sensor internal frame rate was measured by controlling the intensity of the light source. Results are shown in Figure 7, showing the capability of the sensor to adapt to different levels of photon activity.

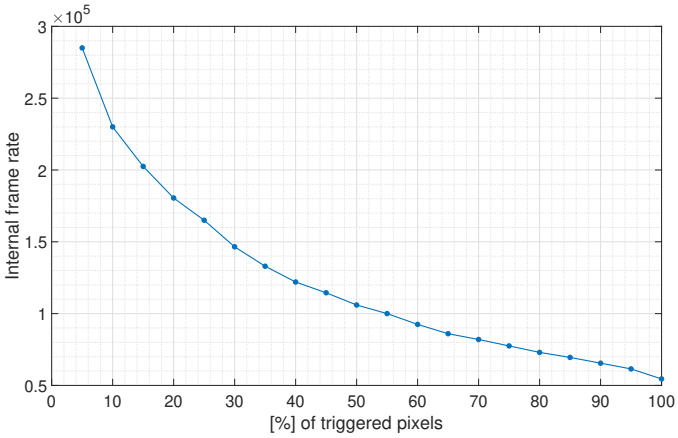

Fig. 7. Measured sensor internal frame rate (thus not considering PC elaboration time) for different number of triggered pixels, demonstrating the capability of the proposed readout scheme to adapt to the level of photon activity.

IV. Conclusion

In this work, a SPAD-based d-ToF linear sensor with the first in-pixel interference rejection capability has been demonstrated. In combination with the dedicated readout architecture, it enables the acquisition of interference-free data with an optimized, adaptive, readout time. The sensor capability to reject interference from other laser sources has been demonstrated in a laboratory setup, as well as the opportunity to use the interference rejection feature on top of the classical photon coincidence to reduce background light to a negligible level, resulting in a measured 42.5 dB interference suppression and up to 23 dB signal gain with a measured data compression ratio of $\simeq$ 98%. The pixel pitch in its actual form factor is not optimized for the evolution into a 2D array and for such reason we envisage a further development with a more compact TDC to extend the proposed pixel architecture into a 2D imager array.

References

[1] M. Perenzoni et al. A 64 × 64-pixels digital silicon photomultiplier direct TOF sensor with 100-Mphotons/s/pixel background rejection and imaging/altimeter mode with 0.14% precision up to 6 km for spacecraft navigation and landing. *IEEE Journal of Solid-State Circuits*, 2017.

[2] P. Padmanabhan et al. A 256×128 3D-stacked (45nm) SPAD FLASH LiDAR with 7-level coincidence detection and progressive gating for 100m range and 10klux background light. In *2021 IEEE International Solid- State Circuits Conference (ISSCC)*, 2021.

[3] E. Manuzzato et al. A 64 × 64-pixel flash LiDAR SPAD imager with distributed pixel-to-pixel correlation for background rejection, tunable automatic pixel sensitivity and first-last event detection strategies for space applications. In *2022 IEEE International Solid- State Circuits Conference (ISSCC)*, 2022.

[4] A. R. Ximenes et al. A 256×256 45/65nm 3d-stacked spad-based direct tof image sensor for lidar applications with optical polar modulation for up to 18.6db interference suppression. In *2018 IEEE International Solid - State Circuits Conference (ISSCC)*, 2018.

[5] H. Seo et al. Direct tof scanning lidar sensor with two-step multievent histogramming tdc and embedded interference filter. *IEEE Journal of Solid-State Circuits*, 2021.